FULL PAPER

An investigation of the on-board microwave radiometer of satellite Altimetry for studying the atmosphere variability

Noor Nabilah Abdullah[1], Dudy Darmawan Wijaya[1*], Irwan Meilano[2], Wedyanto Kuntjoro[1], Zamzam Akhmad Jamaluddin Tanuwijaya[1], Muhammad Rais Abdillah[3] and Fathin Nurzaman[1]

Abstract

Since its first launching, the ability of satellite Altimetry in providing reliable and accurate ocean geophysical information of the sea surface height (SSH), significant wave height (SWH), and wind speed has been proven by numerous researchers, as it was designed for observing the ocean dynamics through nadir range measurement between satellite and the sea surface. However, to achieve high level accuracy, environmental and geophysical effects on the range measurement must be accurately determined and corrected, particularly the effects from the atmospheric water vapor which can divert altimeter range up to 3–45 cm. Thus, satellite Altimetry is originally equipped with the on-board microwave radiometer to measure the water vapour content for correcting the range measurement. To our knowledge, no one has attempted to apply the on-board radiometer for atmospheric studies. In this present work, we attempt to optimize the on-board radiometer data for studying the atmosphere variability due to the El Niño–Southern Oscillation (ENSO) phenomena. We convert the on-board water vapor data into the precipitable water vapour (PWV), and we then investigate whether the derived PWV can capture the variability of ocean–atmosphere phenomena due to ENSO as accurate as the conventional Altimetry-derived sea level anomaly (SLA). Based on our analysis using the empirical orthogonal function (EOF), the results show convincing argument that Altimetry-derived PWV are reliable in examining the atmospheric fluctuation as the correlation of its primary principal component time series (PC1) with Oceanic Nino Index (ONI) is higher (0.87) than SLA (0.80). These results may reinforce the confidence in the ability of satellite Altimetry for ocean–atmospheric studies.

Keywords Sea level, Precipitable water vapour, Satellite Altimetry, Ocean–atmosphere interactions

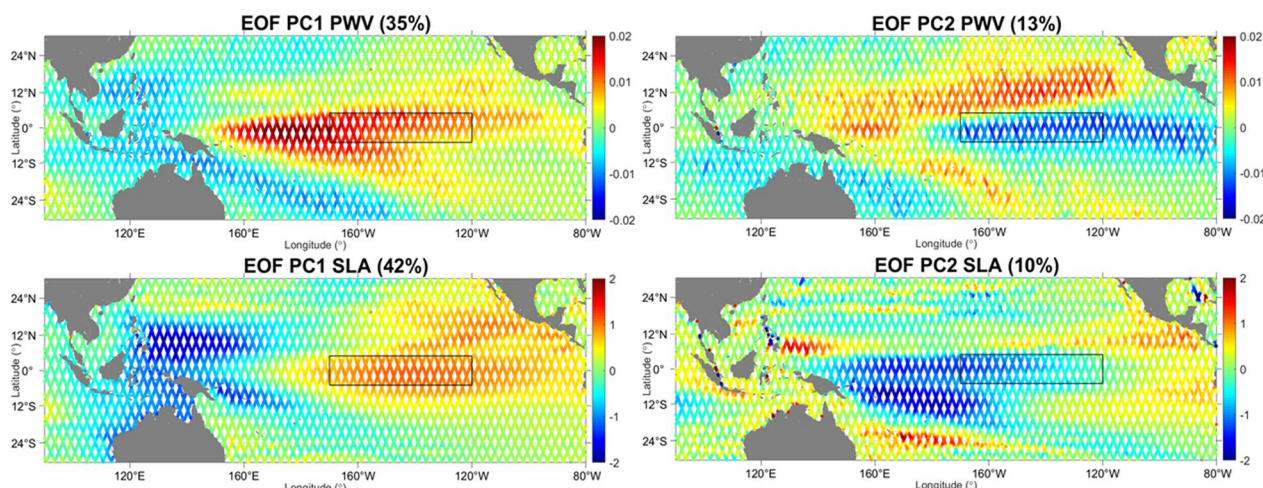*Correspondence:
Dudy Darmawan Wijaya
dudy.wijaya@itb.ac.id
Full list of author information is available at the end of the article

---

Graphical Abstract

Principal Component Analysis (PCA) for PWV and SLA Derived from Altimetry Satellite in Pacific Ocean

*Black rectangles indicate ENSO 3.4 region

Introduction

During the last three decades of radar Altimetry development, the milestones marked not only in monitoring and understanding ocean dynamics at mesoscales level and greater, but also in the study of coastal oceanography, inland water hydrology, and climate have surpassed expectations (Abdalla et al. 2021). It has been ascertained to be a valuable tool in providing ocean geophysical information of sea surface heights (SSHs), significant wave heights (SWHs), wind speed, etc. As reported in numerous researches, the accuracy of Altimetry satellite in measuring sea level variation is up to 2–3 cm in the open ocean and up to 4 cm in the coastal region with the latest missions and retracking algorithms (Shum et al. 1995; Gómez-Enri et al. 2008a, 2008b; Valladeau et al. 2012; Abdullah et al. 2016; Cipollini et al. 2016; Abdullah 2018).

As the accuracy and precision of the altimeter measurements have significantly evolved, ocean variables, particularly sea level, derived from satellite Altimetry are utilised to study the signature of interannual, intra-annual, and seasonal hydro-meteorological phenomena, for instance, Indian Ocean Dipole (IOD) and El Niño–Southern Oscillation (ENSO) (Srinivas et al. 2005; Aparna et al. 2012; Sreenivas et al. 2012; Moon et al. 2015; Cheng et al. 2016; Lyu et al. 2017; Wang et al. 2018; Hamlington et al. 2020), Madden–Julian

Oscillation (MJO) (Zhang et al. 2009; Oliver and Thompson 2010, 2011; Rohith et al. 2019), and winter and summer monsoons (Chen et al. 2010; Saramul and Ezer 2014; Trott and Subrahmanyam 2019; Qu et al. 2022).

The primary trigger for these hydro-meteorological events is the complex interaction (coupling) between the atmosphere and ocean variabilities (Gupta et al. 2009; Jayawardena 2015; Debele et al. 2019), that is generally due to the interchange energy of solar radiation at the overlapping boundary of the atmosphere and the ocean (Fedorov 2008; Xie 2009; Misra 2014). While the influence of ocean–atmospheric coupling to the ocean part has been proven to be well perceived through satellite altimeter-derived sea level, the atmospheric part is yet to be elaborated. According to the latest technology of satellite Altimetry, we believe that the satellite is capable to provide reliable data not only for the ocean dynamics, but also for the atmosphere. This is because satellite Altimetry is not only equipped with the radar system to measure the sea surface, but also it is equipped with the microwave radiometer to measure atmospheric water vapour. The radiometer measurement initially provides the wet path delay correction for the main altimeter range measurement (Eymard et al. 1994; Blanc et al. 1996; Fernandes et al. 2015, 2021). This perspective develops a new potential for satellite Altimetry to also be exploited to observe

Abdullah *et al. Earth, Planets and Space*   (2024) 76:34

Page 3 of 19

the atmosphere. However, study regarding the employment of altimeter microwave radiometer for atmosphere observation is still limited, albeit the effort to improve the accuracy of the satellite Altimetry microwave radiometer has been a focus on several research since the wet path delay (path delay caused by tropospheric water vapour) has a significant effect on Altimetry range measurement. The uncertainty of wet path delay or wet tropospheric correction (WTC) from Jason-1 radiometer measurement is approximately 0.74 ± 0.15 cm (Brown et al. 2004). Apart from that, the accuracy of microwave radiometer measurement has been enhanced on each follow-on satellite mission (Brown 2010; Maiwald et al. 2016; Fernandes and Lázaro 2018). With this accuracy, the benefit of radiometer measurement should be acknowledged, not only to provide correction for the altimeter range, but also for the purpose of the atmosphere observation. Thus, the aim of this present study is to investigate the applicability of the on-board radiometer in studying the interannual ocean–atmospheric phenomena caused by ENSO and to compare the results against those derived from the sea surface measurements in the form of sea level anomaly (SLA).

The research area selected for this study is the Pacific Ocean as it has significant influence on climate variability, particularly over equatorial zone. In the interannual timescale, the ocean and atmosphere variability in the Pacific Ocean are predominantly influenced by anomalous climate mode of ENSO, which involves non-periodic fluctuation in winds, sea surface temperatures (SST), and air pressure of the underlying atmosphere (Southern Oscillation) across the equator over the tropical eastern Pacific Ocean (Philander 1985; Holton and Dmowska 1989; Timmermann et al. 2018). In addition, this area is selected because there are numerous previous studies on that area which can thoroughly validate our results, as the primary aim of this study is merely to investigate the applicability of the on-board microwave radiometer to capture the atmospheric variability during ocean–atmosphere phenomena (in this case ENSO). It is not intended to elaborate a new physical signature of the event.

ENSO phenomenon relates to walker circulation due to the forces of pressure gradient caused by high-pressure area over the eastern Pacific and low-pressure system over Maritime Continent (Wang et al. 2000; Chang et al. 2004; Zhang et al. 2016). La Niña is caused by an extremely strong walker circulation, which results in colder ocean temperatures in the central and eastern tropical Pacific Ocean, owning to enhanced upwelling. During this phase, the trade winds are stronger, resulting warmer ocean temperature over western Pacific Ocean. Deep convection is more concentrated in Indonesia, thus resulting heavy rainfall over the region. At a certain point,

the walker circulation experience weakening or reversal (which comprises trade winds), causing the upwelling of cool deep-sea water to dwindle or vanish. This situation causing the sea surface to reach temperatures above average, thus creating El Niño. During this phase, when the trade wind anomalously is weak, the sea temperature over the eastern part become warm. Thus, the deep convection of walker circulation moves to the east, resulting lower precipitation in Indonesia.

This phenomenon has major influence over the tropics and subtropics climates, particularly when this oscillations pattern become extreme (Wang et al. 2000; Chang et al. 2004; Han and Huang 2009; Zhang et al. 2016). It causes intense weather, such as floods and droughts in several regions in the world. Regions bordering the Pacific Ocean are the most affected, causing major problems particularly to the developing countries that depend on agricultures (e.g., Garden 2014; Chang-Yang et al. 2016; Luo and Lau 2020; Qian et al. 2020) and fisheries (e.g.,Salinger 2013; Kumar et al. 2014; Lehodey et al. 2020) as part of their economic resources.

This paper is divided into four Sections. Sect. "Introduction": Introduction is an introductory section which discusses the primary premise of the research, including the aim and expected outcomes of this study. Sect. "Data and Methodology": Data and Methodology explains the attributes of Altimetry data used, including the observation period and missions involved. This section also includes the procedure used in deriving Altimetry-derived SLA and PWV anomalies. Sect. "Results and discussions": Results and discussion provides deliberate analysis and discussion regarding the variability of SLA and PWV during ENSO and the interrelation between those variables in the Pacific Ocean. Sect. "Conclusions and remarks": Conclusion and Remarks summarises the findings of the research. The expected progress in the future study using Altimetry data for ocean–atmosphere interrelation are also discussed.

Data and methodology
Altimetry data base

The data of 30 years from January 1993 to December 2022 from five (5) satellite missions: TOPEX, Jason-1, Jason-2, Jason-3, and Sentinel-6a are utilised to derive SLA and PWV. The timeline of all missions is shown in Fig. 1. The data are retrieved from Radar Altimeter Database System (RADS) and Archiving, Validation, and Interpretation of Satellite Oceanographic data (AVISO). The temporal resolution of the data is 9.9 days and the sampling interval along track is ~ 6 km. The details description of the satellite's tracks geometry is provided in Table 1. The spatial map of the study area including satellite passes used in the study and highlighted passes and points used
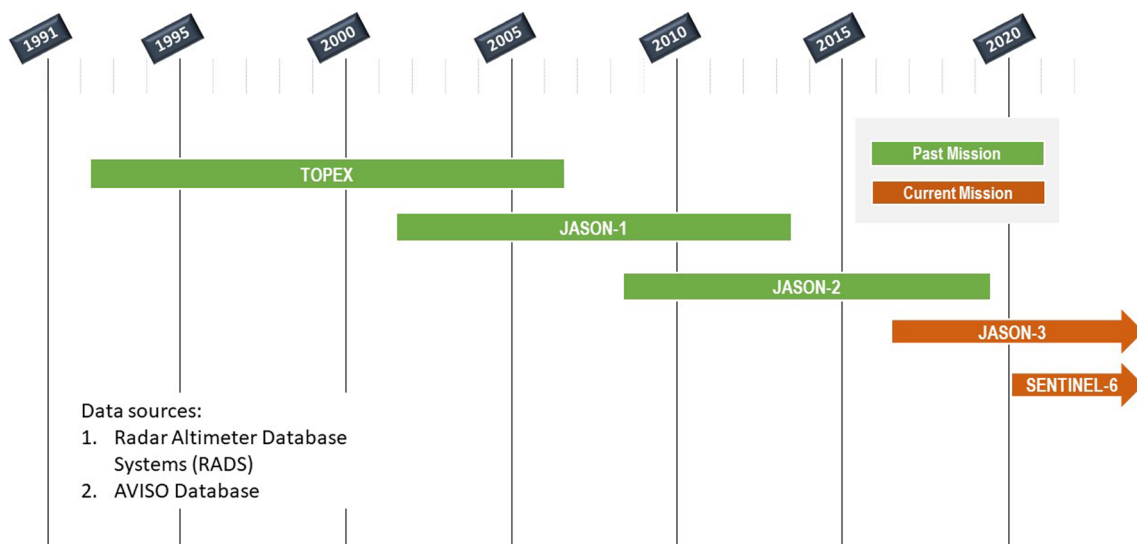
**Fig. 1** Timeline of satellite Altimetry missions used in the study

Table 1 Characteristics of orbit parameters for TOPEX, Jason-1, Jason-2, Jason-3, and Sentinel-6

Main characteristics	
Ground track separation at Equator	315 km
Along-track sampling interval	~6 km
Number of passes per cycle	254
Number of passes used in this study	149
Number of 1 Hz measurements used in this study	184,933
Orbital velocity	7.2 km/s
Ground scanning velocity	5.8 km/s
Repeat cycle	9.9 days

in across equator and along equator analysis, respectively, are indicated in Fig. 2. The derivations of SLA and PWV are provided in Sect. "Altimetry-derived SLA" and Sect. "Altimetry-derived PWV", respectively.

Altimetry-derived SLA

The basic concept of satellite altimeter operation is to measure height or distance between the satellite and the sea surface using a nadir pointing microwave instrument called Radar Altimeter (Gommenginger et al. 2011). The measured distance (called "the range") is then used to determine the value of sea surface height (SSH), which
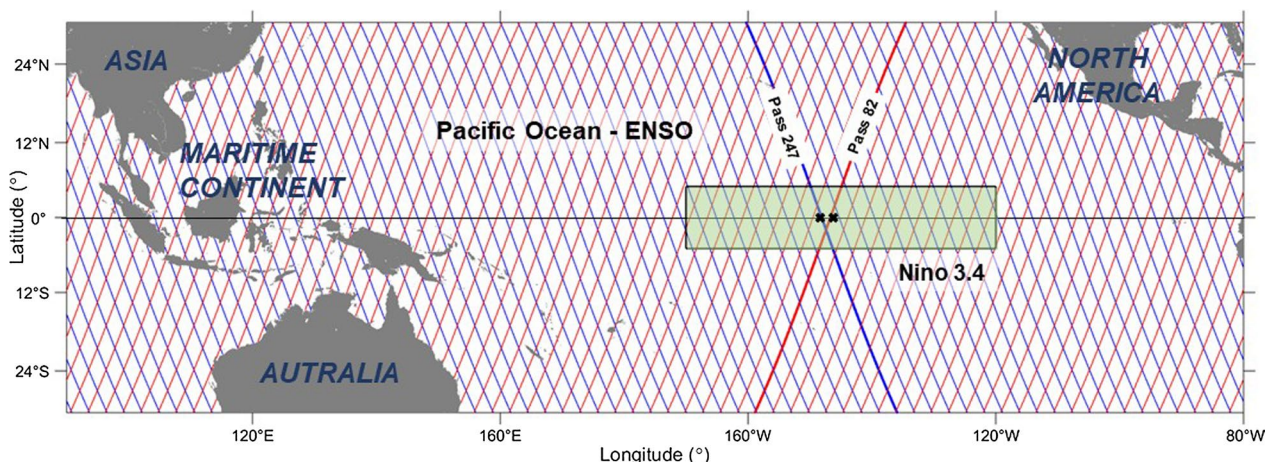
Fig. 2 Region of study area. The green rectangle indicates the Nino 3.4 region where ONI is computed. Red lines indicate the ascending passes and blue lines indicate the descending passes. Passes 127 and 88 are used for along track analysis and black marks are the point used as example for time-series plot

is the height between the instantaneous sea surface and reference ellipsoid, by computing the different value between the satellite position and the measured distance. Meanwhile, SLA is defined as the height between the instantaneous sea surface and mean sea surface height (MSS). The distinction between SSH and SLA is described in Fig. 3.

SLA from satellite Altimetry range measurement can be extracted as in the following equation (Andersen and Scharroo 2011):

$$h_{SLA} = H - R_{retracked} - \Delta h_{dry} - \Delta h_{wet} - \Delta h_{iono}$$
$$- \Delta h_{ssb} - h_{MSS} - h_{tides} - h_{atm}$$
(1)

where H is the satellite altitude above reference ellipsoid. $R_{retracked} = c\frac{t}{2}$ is the computed range from travel time, t, observed by altimeter radar, and c is the speed of light. $R_{retracked}$ is corrected observed range using waveform retracking algorithm, MLE-3 (Thibaut et al. 2010). Δh_{dry} is dry tropospheric correction, Δh_{wet} is wet tropospheric correction, Δh_{iono} is ionospheric correction, Δh_{ssb} is seas state bias correction, h_{MSS} is mean sea surface height, h_{tides} is tide corrections (including ocean tide, solid earth tide, pole tide, and tide loading) and h_{atm} is dynamic atmospheric corrections (including high frequency fluctuation and inverse barometer correction). Details about the corrections and models used to derive SLA are tabulated in Table 1.

Altimetry-derived PWV

The on-board microwave radiometer is used to derive three main elements in the atmosphere: water vapour, cloud liquid water, and wind driven variations on sea surface by collecting the radiations that are reflected by the ocean. These elements are utilised to derive wet tropospheric delay for range measured by altimeter radar.

The retrieval of wet tropospheric delay or correction, R_{wet}, involves two processing stages. The first stage is to calibrate the output of brightness temperatures and to remove any correlation between the hardware physical temperature and the brightness temperatures, which includes: (*i*) the correction of hardware losses from the system component to attain the antenna temperature and (*ii*) the elimination of on-earth and off-earth side lobe contamination from the antenna temperature to get the brightness temperatures (Brown et al. 2004). The second stage is to retrieve the wet tropospheric correction from brightness temperatures. It begins with the following equation for estimating cloud liquid, L_z, and wind speed, W, from brightness temperatures (Keihm et al. 1995):

$$L_z = l_0 + \sum l_f T_b(f)$$
(2)
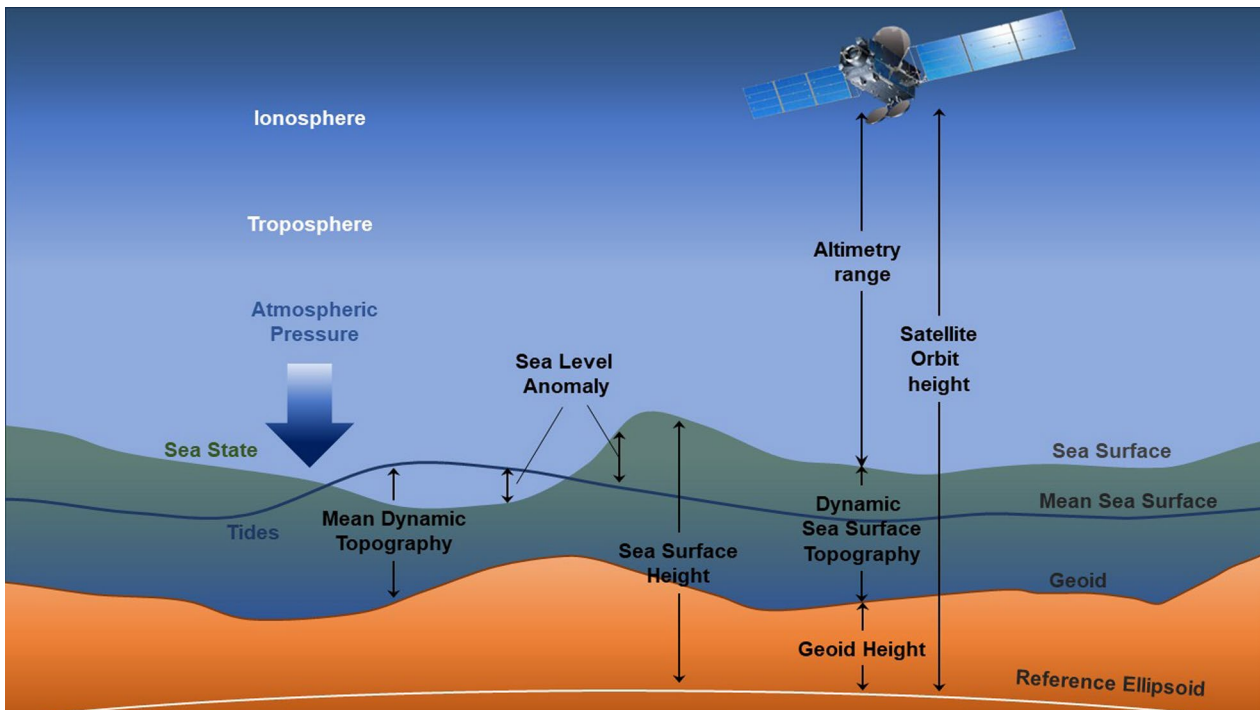
Fig. 3 Principal of satellite Altimetry observation. Note that the altitudes are not to the scale

$$W = w_0 + \sum w_f T_b(f) \tag{3}$$

where $T_b(f)$ is the measured brightness temperature corresponding to the frequency, f, and l_0, l_f, w_0, and w_f are predetermined coefficients.

Subsequently, the path delay induced by water vapour is retrieved through two-step statistical inversion. The first step is computation of the initial estimate of the path delay value, $PD^{(1)}$, using coefficients associated with wind speed, which can be expressed as

$$PD^{(1)} = B_0^{(1)}(w) \sum B_f^{(1)}(w) * \ln\left[280 - T_b(f)\right] \tag{4}$$

where $B^{(1)}$ are coefficients for the initial value associated with wind speed. The second step is computation of the final path delay value, $PD^{(2)}$, using coefficient associated with wind speed and the initial path delay value, and can be expressed as

$$PD^{(2)} = B_0\left(w, PD^{(1)}\right) + \sum B_f\left(w, PD^{(1)}\right) * \ln[280 - T_b(f)] \tag{5}$$

where B as coefficient of final value associated with wind speed and the initial path delay value. Thus, the total wet path delay, WPD, can be obtained by adding the cloud liquid component to the final path delay value, as shown in Eq. (6). The wet tropospheric correction, R_{wet}, which is a negative value of WPD is estimated in Eq. (7):

$$WPD = PD^{(2)} + 1.6 * L_z \tag{6}$$

$$R_{wet} = -WPD \tag{7}$$

The acquired R_{wet} value can then be used to compute the total water vapour concentration in a specific atmospheric column, referred to as PWV, as expressed in the following equation (Fernandes et al. 2021):

$$PWV = \frac{10^6}{\rho R_v\left(\left(\frac{k_3}{T_m}\right) + k_{2'}\right)} * R_{wet} \tag{8}$$

where $R_v = 4.61527 m^3/kg.K$ is the specific gas constant for the water vapour, $\rho = 997 kg/m^3$ is the density of water, $k_3 = 3.7765 * 10^{-5} K^2/mbar$, $k_{2'} = 17 K/mbar$, and T_m is the mean temperature of atmosphere. Since T_m is not recorded by the altimeter satellite, its value is acquired using existing Global Pressure Temperature (GPT) model. This model is retrieved from European Centre of Medium Range Weather Forecast reanalysis v5 (ECMWF ERA5), which is able to provide yearly data variation from earth pressure and temperature (Böhm et al. 2007). As the T_m data are provided in a grid format with 1° resolution, meanwhile, the altimetry data used are

along track data, T_m values are interpolated using linear interpolation to the altimetry observation points. The period of T_m is also similar to the altimetry observation period.

Please note that, for Jason-1, Jason-2, and Jason-3 satellite missions, atmosphere water vapour content data are provided in the raw satellite data file in unit kg/m² and final PWV can be simply calculated by multiplying the data with water density value. However, for TOPEX and Sentinel-6a satellite missions, the data are not included in satellite data file, instead it is provided as wet tropospheric correction, R_{wet}. Therefore, to standardise the data, R_{wet} is used to derive PWV for all missions.

R_{wet} has been through thorough validation using multiple independent data sets, including GNSS-derived path delay (Fernandes et al. 2010), European Centre for Medium-Range Weather Forecasts (ECMWF) Atmospheric Model, Global Precipitation Measurement (GPM), etc. (Fernandes et al. 2015; Fernandes and Lázaro 2018). With the significant works the accuracy of wet tropospheric correction nowadays is up to 1–3 cm (Fernandes et al. 2021).

Extraction of inter-annual signal

To effectively analyse the Walker Circulation that associates with interannual phenomena (in this case, ENSO), annual harmonics and dominant climatology component for inter-seasonal phenomena must be eliminated from SLA and PWV time series, to retrieve the variables' anomaly.

As these inter-seasonal components depict the homogenous state without anomalous variation, they can be modelled by averaging long period data. The modelled components are the long-term mean and trends, and frequent seasonal oscillation for each variable, using the following equations:

$$\nabla M(t) = M(t) - \overline{M} - T(t) - S(t) \tag{9}$$

where ∇M is the variable anomaly, t is time, M is the variable observed values, $\overline{M}$ is the variable long term mean, T and S are the trend and seasonal components of the variable time series, respectively. The elements for the trend and seasonal components are estimated using simple least square adjustment. The trend component is determined using the simple linear model and the seasonal component is determined by the first three harmonics of the annual cycle. T and S can be defined as follows:

$$T(t) = a_{tr} + b_{tr}t \tag{10}$$

$$S(t) = \sum_{k=1}^{3} (a_k \cos(k\omega t) + b_k \sin(k\omega t)) \tag{11}$$

where a_{tr} and b_{tr} are the constant and the gradient term of the linear trend component, respectively. ω is the frequency of 1 year, which can be defined as $\frac{2\pi}{365.25day^{-1}}$; thus, a_k and b_k for $k = 1, 2, \&3$ are sine and cosine terms for the first three harmonics of the annual cycle. The period of data to resolve these components using least square adjustment is 30 years (January 193 to December 2022). The exact round number of years for the base period is necessary to minimise bias from non-complete annual harmonics cycle. However, decadal signals are neglected in the modelling and remain in the time series, as their oscillations are insignificant and has not influence the pattern of interannual variability.

To analyse the influence of interannual phenomena to the SLA and PWV variabilities, for instance, ENSO, annual harmonics and dominant climatology component are eliminated from SLA and PWV time series. Subsequently, simple average is performed to extract monthly data from all the available data observed in the respective month. The seasonal signal modelling and elimination are applied to all observed data in all 1 Hz

altimeter observations used in the study. Figure 4 shows the derived SLA and PWV time series overlaid with the modelled climatological components, and SLA and PWV anomaly after climatological components have been eliminated from the time series, respectively.

Results and discussion
Validation of altimetry-derived PWV
To determine the capability of Altimetry-derived PWV in capturing the state of water content in the atmosphere, PWV derived from ECMWF ERA5 WTC model is used to validate the Altimeter-derived PWV. This ECMWF ERA5 WTC model is retrieved from AVISO database. T_m used in ECMWF-derived PWV are similar to the values used in Altimeter-derived PWV. The comparison is conducted on every 1 Hz measurements over the study region. Temporal resolution of both data is 9.9 days, corresponding to the Altimeter's temporal resolution. For validation purposes, correlation coefficient between both data sets is computed and histogram of deviation of difference is plotted. The statistical results are indicated in Table 2 and Fig. 5.
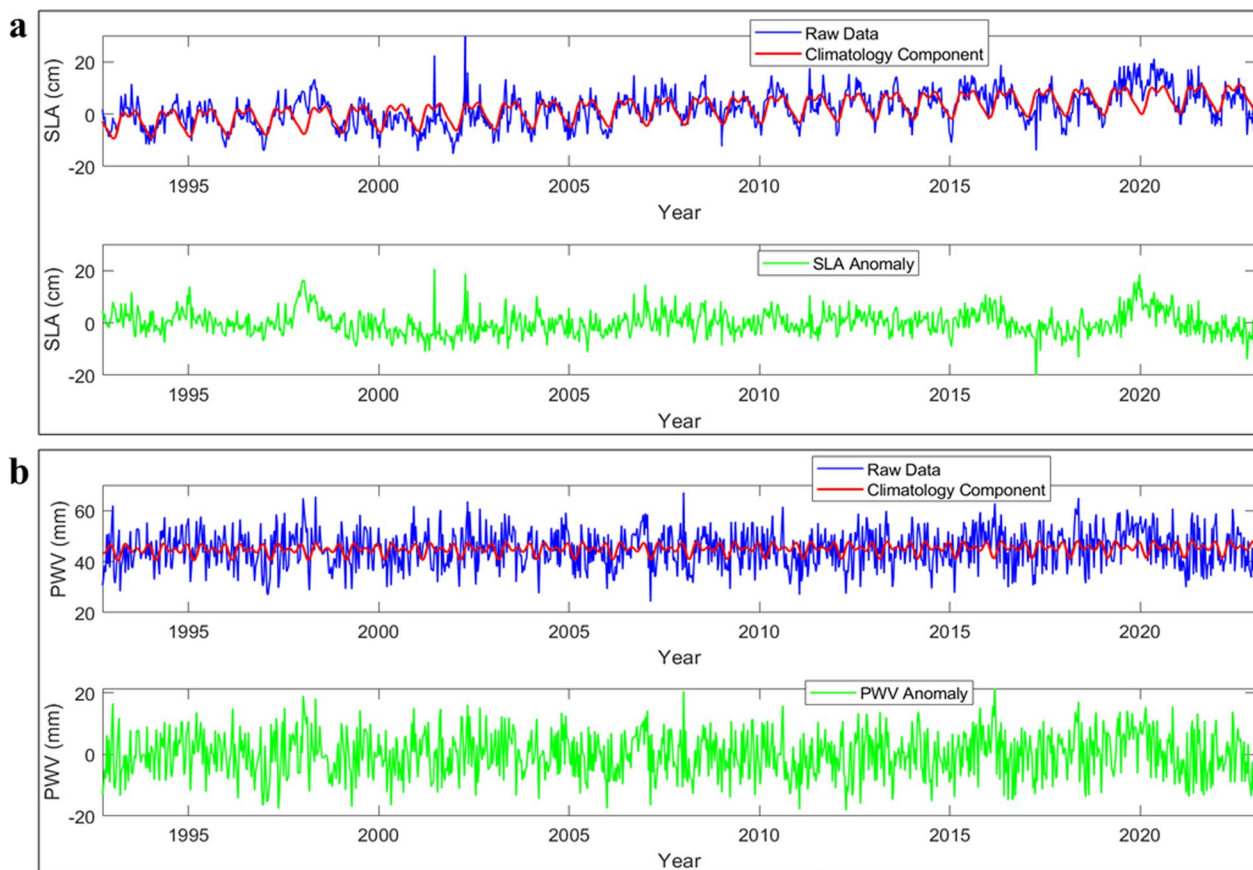
Fig. 4 Example of the time series of raw data overlapped with the estimated climatology components and anomaly (raw data minus climatology) for SLA (**a**) and PWV (**b**) at a point located at ENSO 3.4 region

Abdullah *et al. Earth, Planets and Space*   (2024) 76:34

Page 8 of 19

Table 2 Statistical results of comparison between Altimetry-derived PWV and ECMWF-derived PWV

Main characteristics	Values
Correlation coefficient	0.976
Mean difference	0.371 mm
Standard deviation of difference	2.518 mm
Root mean square difference	2.518 mm
Normalised root mean square difference	1.011 mm

There is a high positive correlation between the two data sets which yields correlation coefficient value of 0.976, showing that Altimetry-derived PWV is in a good agreement with ECMWF-derived PWV. The Root Mean Square Difference (RMSD) is 2.545 mm and the normalised (NRMSD) or the ratio of the RMSD to the standard deviation of difference (STDD) is 1.011 mm. The RMSD values indicate that the discrepancy between both data sets is insignificant. From the histogram of the difference (Fig. 5b), the difference appears to be normally distributed with the symmetrical bell shape. The peak value is close to zero, signifies that the mean differences are extremely small. The discrepancies are probably caused by random error (e.g., sensor noise, electromagnetic interference, etc.) rather than error in derivations or caused by inaccurate data.

Variability of SLA and PWV during El Niño and La Niña

The intensity of ENSO is defined by the Oceanic Nino Index (ONI), which the average of 3 months of ocean SST anomaly in the central tropical Pacific (5°N–5°S, 120°–170°W). El Niño and La Niña conditions are considered to be present when the ONI is higher than 0.5 and lower than −0.5, respectively, which is warmer and cooler than average. Figure 6 depicts the variation of PWV and SLA from lower to upper latitude for ascending (Pass 82) and descending (Pass 247) passes derived at ENSO region. The PWV and SLA are plotted during different phases of ENSO (El Niño, neutral, and La Niña). The fluctuations of both variables are associated with ONI as it increases (decreases) during high ONI (low ONI) approaching the ENSO region. During the extreme El Nino with ONI value up to 2.71, the anomalies of PWV and SLA in the central Pacific increase up to 15 mm and 17 cm, respectively. Conversely, during La Nina event with negative ONI value −1.77, PWV and SLA anomalies in the central Pacific decrease down to approximately -8 mm and -9 cm, respectively. Compared to the natural condition when ONI value −0.01,
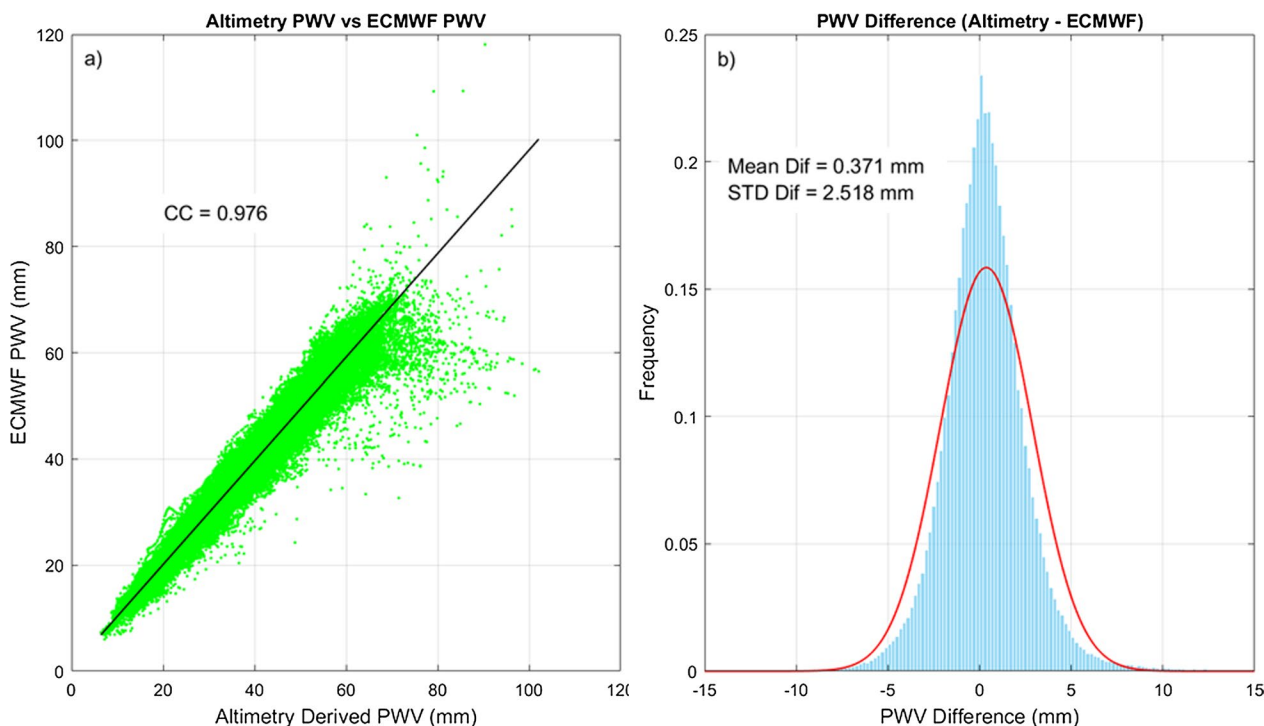
Fig. 5 a Scatter plot of monthly average Altimetry-derived PWV and ECMWF PWV over study area. **b** Histogram of PWV difference between Altimetry-derived PWV and ECMF-derived PWV in the validation area
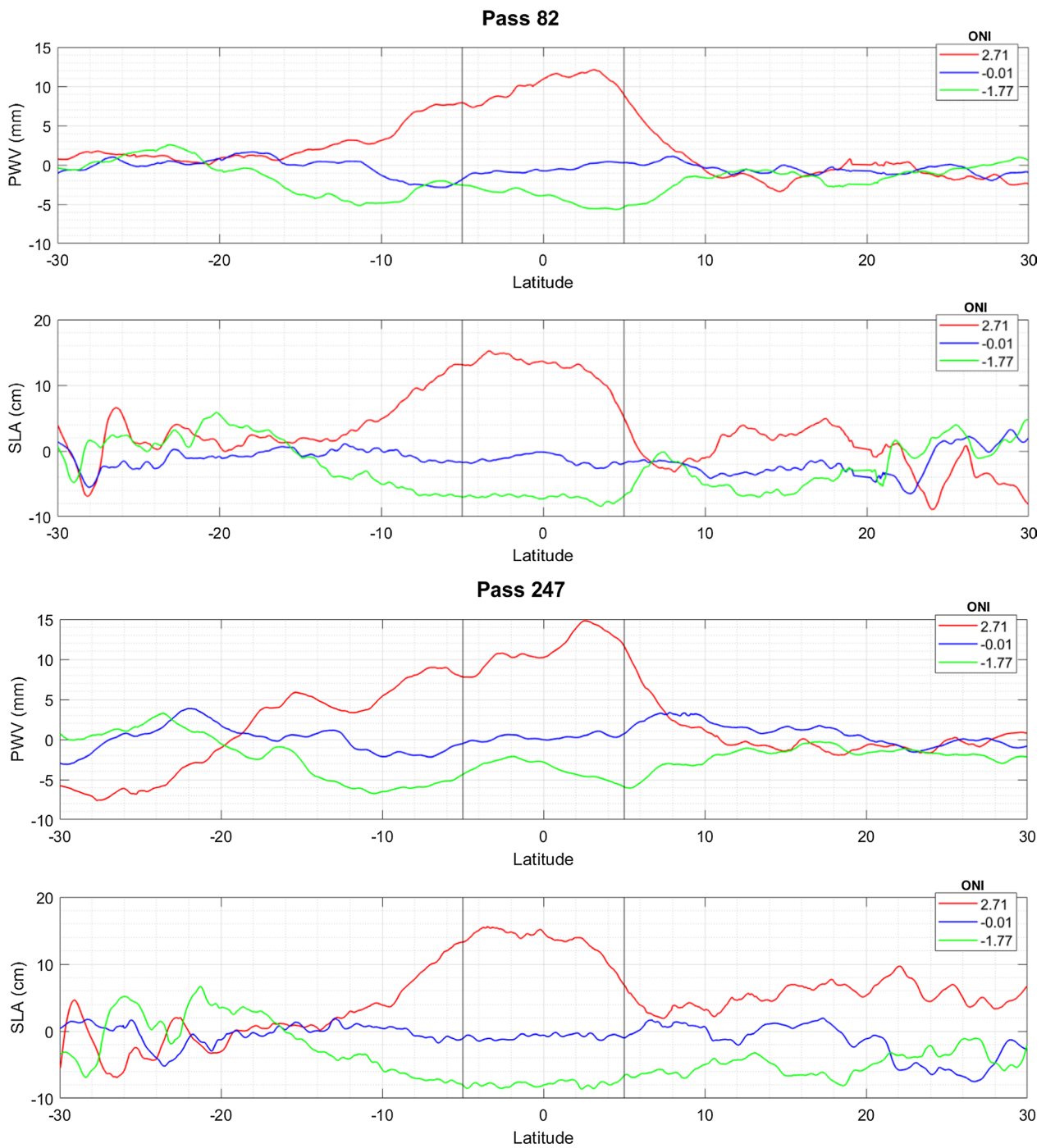
Fig. 6 PWV and SLA across ENSO 3.4 region for pass 82 (ascending) and pass 247 (descending) during three different phases of ENSO determined by ONI

the PWV and SLA anomalies are insignificant. The initial results evidently indicate that both PWV and SLA variables sensitive to ENSO, hence the variables can be further exploited to investigate the ocean–atmosphere interactions.

Theoretically, a walker circulation during ENSO season upholds an equilibrium state in the tropical ocean and atmosphere, in which during El Niño the eastern Pacific Ocean is characterised by higher sea level and

deeper thermocline as the atmospheric pressure is low. Low atmospheric pressure is driven by relatively increasing precipitation (Ji et al. 2000; Lau and Yang 2003; Tsonis et al. 2003; Gastineau et al. 2009; Stuecker et al. 2017). Whereas, in the Maritime Continent (western Pacific Ocean), the sea level is lower as the

atmospheric pressure is higher resulted from decreasing precipitation. The opposite situation occurs during the La Niña season (Chang et al. 2004; Jia et al. 2016; Zhang et al. 2016). These patterns are apparent in the spatial plot of Pacific Ocean in Figs. 7 and 8, which depict the variation of PWV and SLA during the highest, neutral,
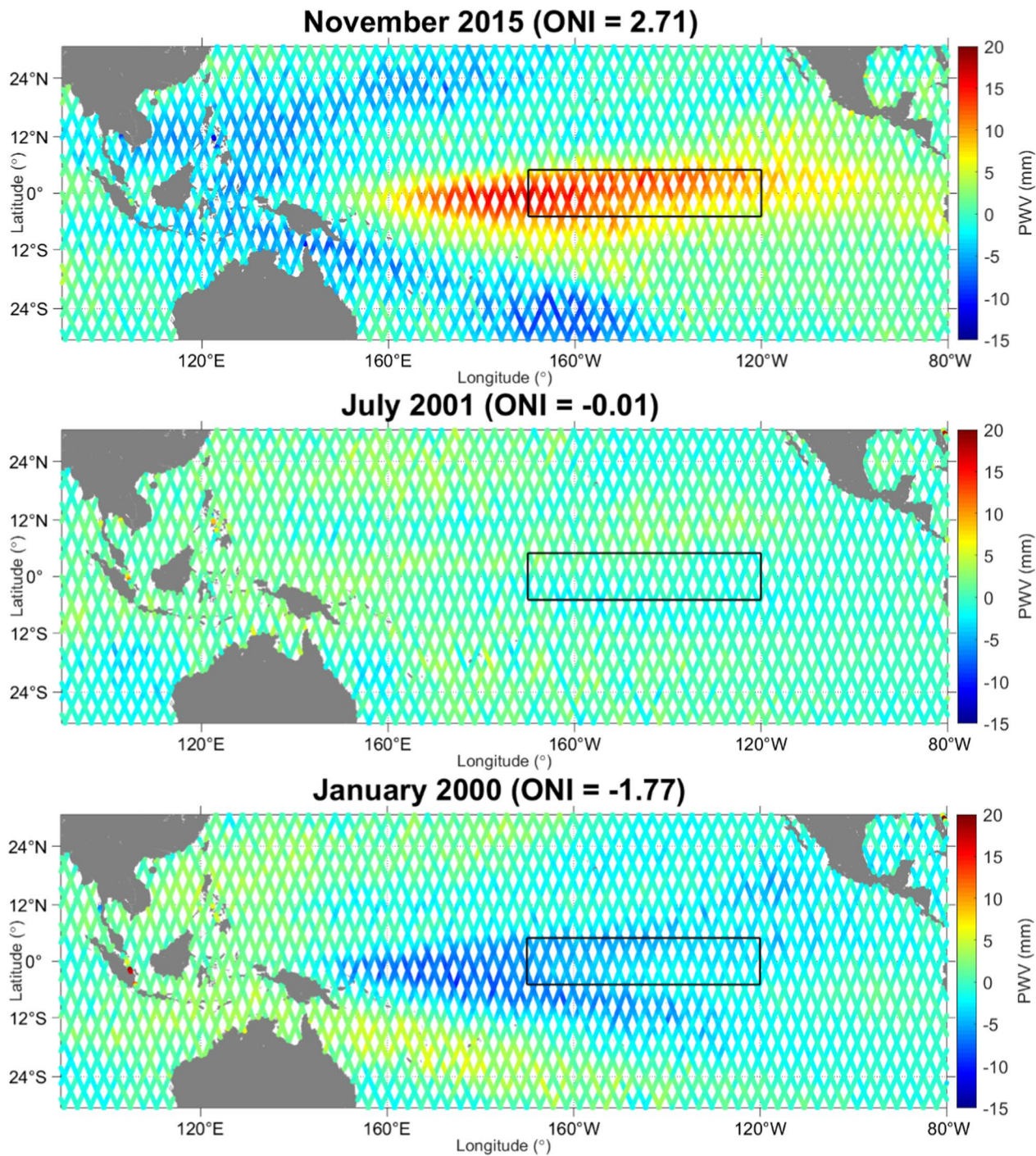
Fig. 7 Spatial map of anomaly PWV during three different phases of ENSO determined by ONI. The rectangular block shows the ENSO 3.4 region
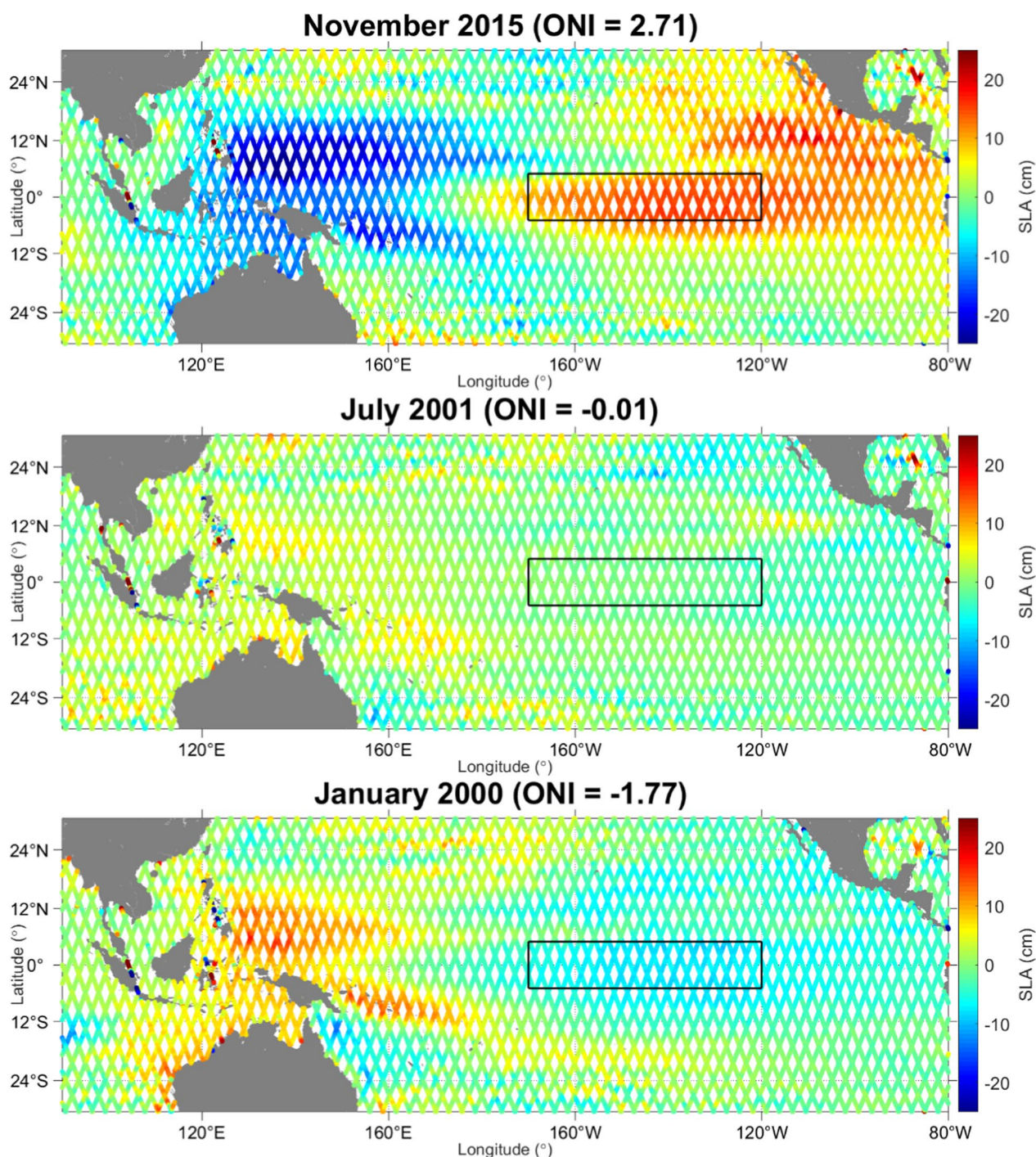
Fig. 8 Spatial map of anomaly SLA during three different phases of ENSO determined by ONI. The rectangular block shows the ENSO 3.4 region

and lowest ONI. The pole like gradient of SLA is more significant during both El Niño and La Niña seasons. During the El Niño the SLA anomalies increase up to 23 cm over centra Pacific and decrease down to −25 cm over western Pacific. On the contrary, during La Niña, the SLA anomalies increase up to 22 cm in the western

Pacific and decrease down to −16 cm over the centra Pacific. Meanwhile, for PWV, the gradient creates basin like pattern where the highest anomalies during the El Niño event increase up to 18 mm along the equator in the Central Pacific and decrease down to −14 mm in the region starting from Maritime Continent, spreading to

the upper and lower latitude toward the central Pacific. Similar patter also shown during La Niña with the contradict increasing (up to 9 mm) and decreasing (down to −14 mm) anomalies regions.

Noted that the number of parameters that influence SLA variability are significantly higher than parameters that affect PWV, yielding the different in general pattern throughout the entire study region. However, the main concern is the changes in the convection and subsidence areas of walker circulation during ENSO event, which are in the central Pacific and Maritime Continent. As apparent in the figures, the fluctuation of SLA and PWV anomaly during El Niño and La Niña are similar and highly correlated with ONI (Fig. 9), which is higher than 0.8 and lower than −0.8. As expected, since ONI is determined based on the SST observed in the highlighted region (black box in the figures) over the central Pacific, its correlation with SLA and PWV over this area is positive. As aforementioned, the nature of these variables over the Maritime Continent are contrast with that of in the central Pacific, particularly during extreme events (high and low ONI), resulting in negative correlations with ONI.
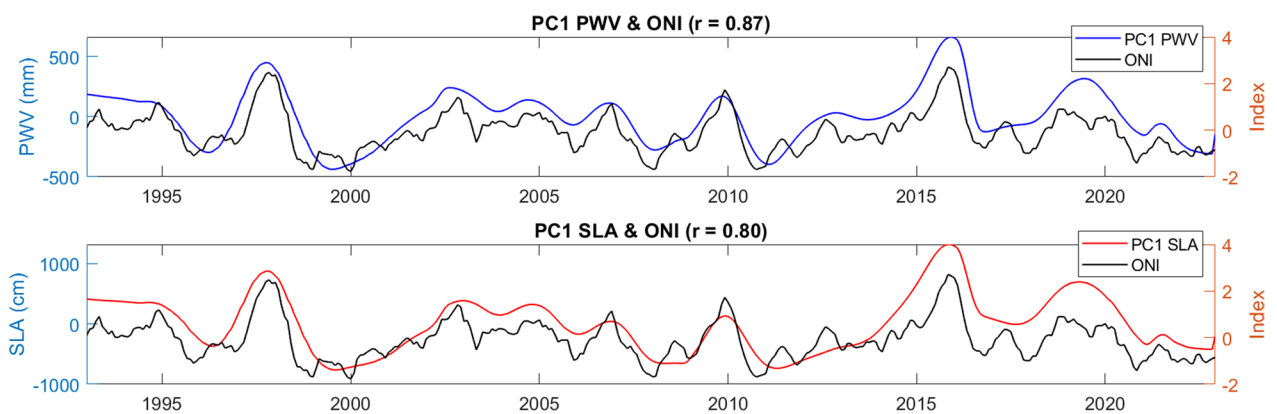
Principal component analysis

A standard Empirical Orthogonal Function (EOF) analysis has been performed on the Altimetry-derived SLA and PWV to identify and discrete the underlying dominant variations from timeseries of both SLA and PWV variables. The primary leading principal component (PC1) for PWV and SLA, which, respectively, explain 35% and 42% of the total variance, have generated significant contrast spatial pattern over central Pacific and Maritime Continent. However, SLA forms a pole like pattern; meanwhile, for PWV, the mode is centred in the central Pacific. According to the spatial patterns, prompt analysis can consider that EOF PC1 of both SLA and PWV are associated with ENSO variability (Fig. 10). The argument is further supported by the high correlation coefficient of both PWV and SLA correspondent time series PC1 with ONI, which are 0.87 and 0.80, respectively (Fig. 11).
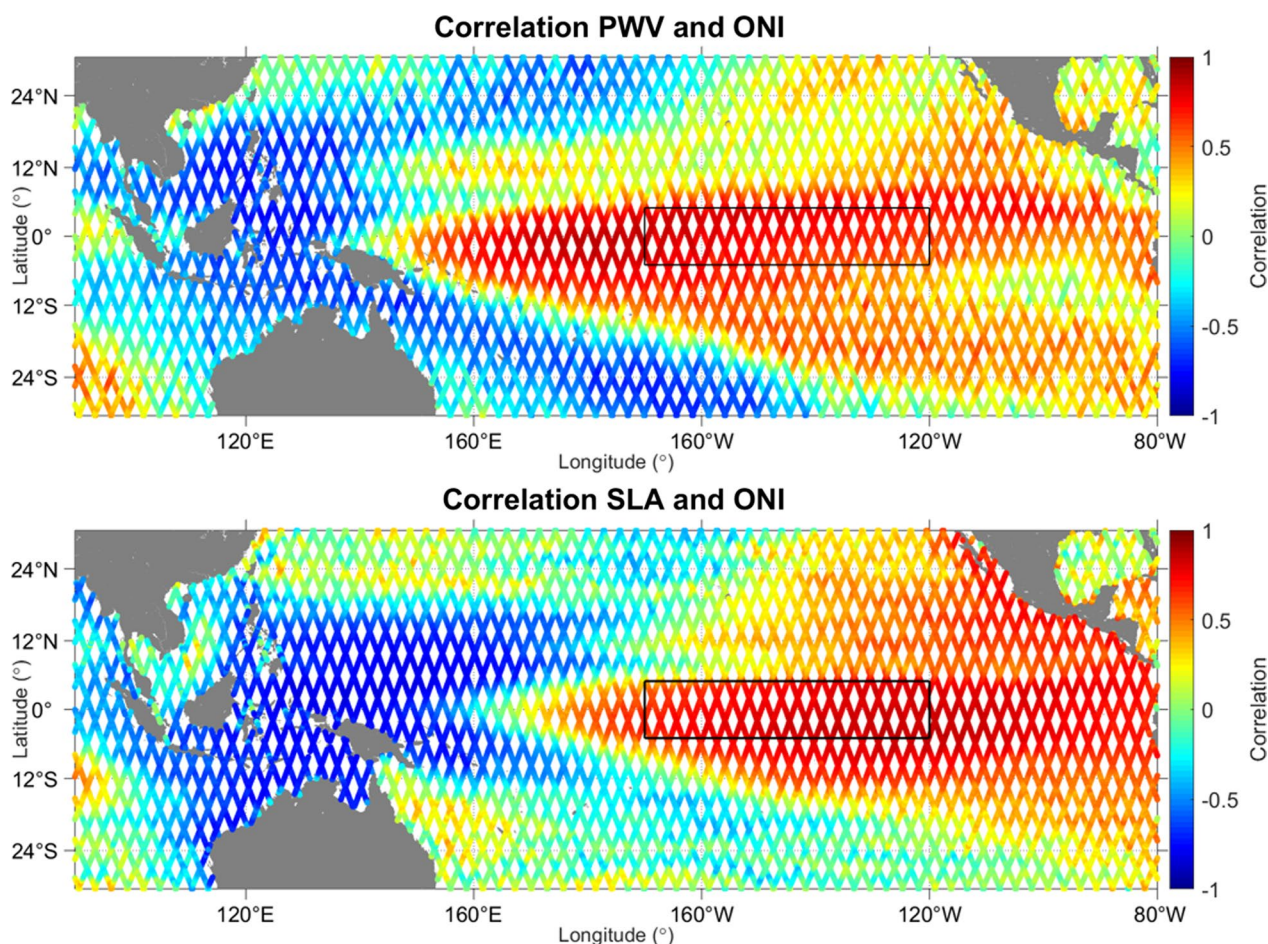
Fig. 9 Spatial map of correlation coefficients between PWV (top) and SLA (bottom) with ONI for 30 years along track data over Pacific Ocean
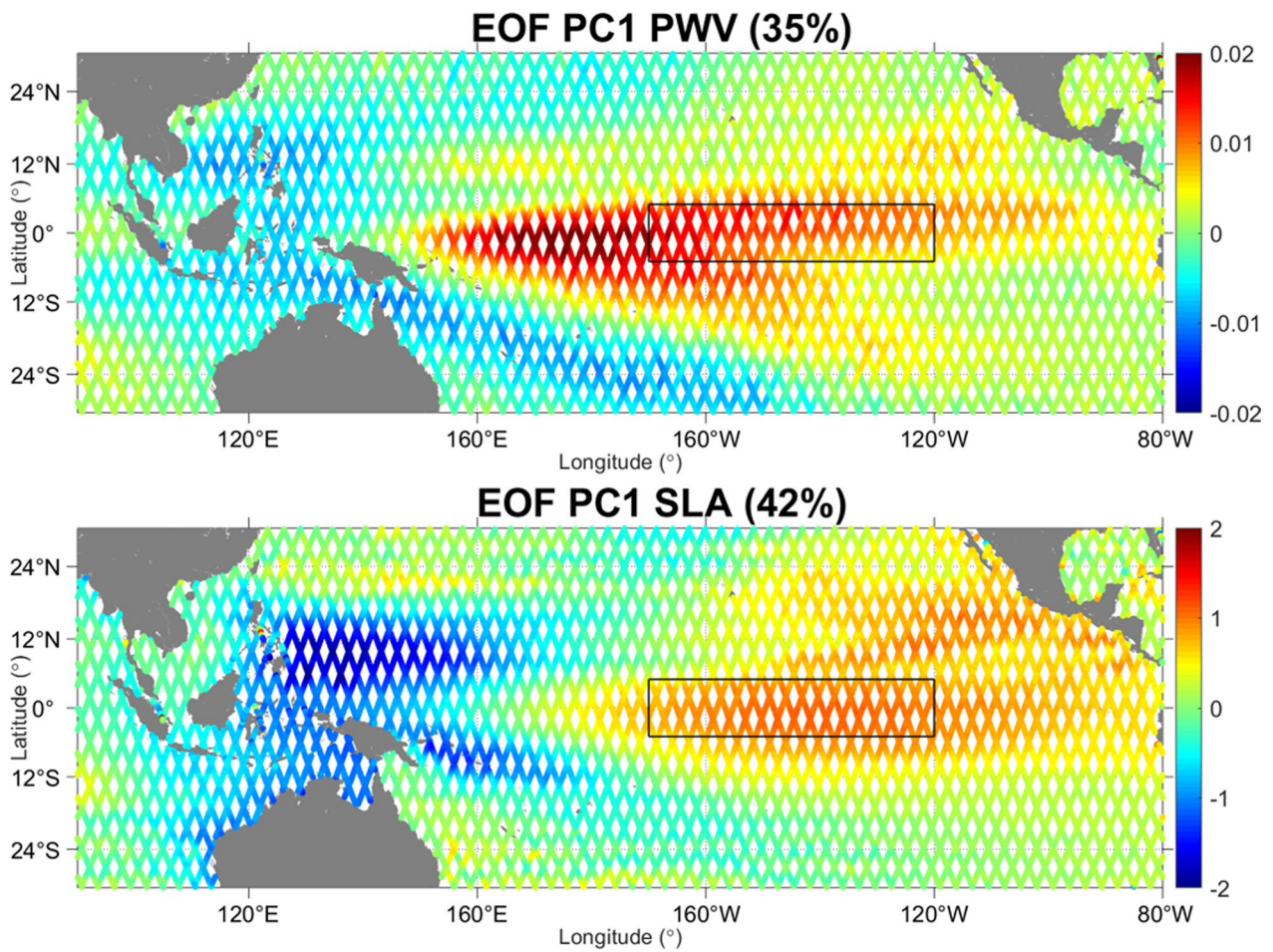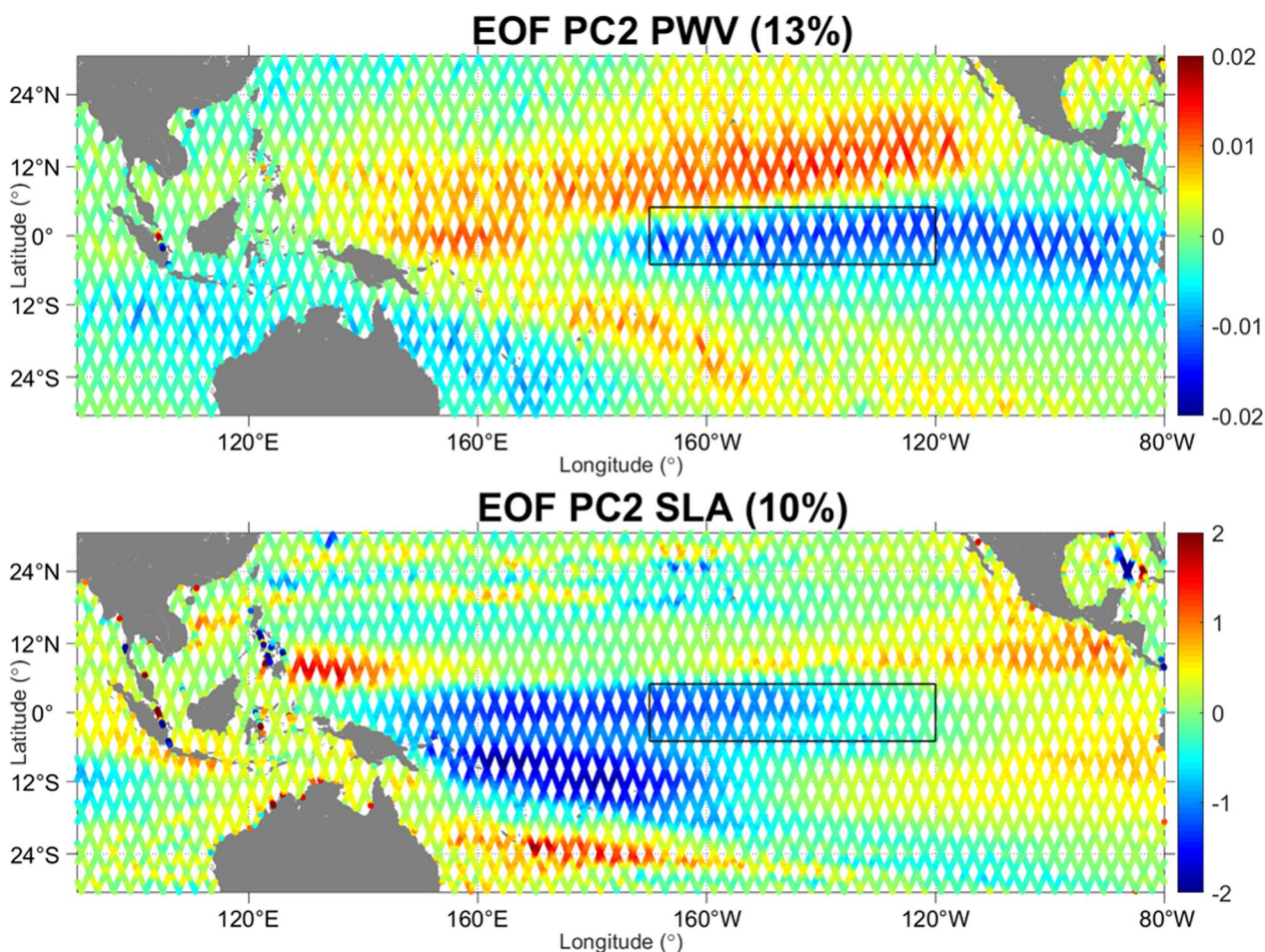
Fig. 10 Principal loading map of primary principal component from EOF analysis on the Altimetry-derived PWV (top) and SLA (bottom) for along track data over Pacific Ocean

Fig. 11 Time series of primary principal component for Altimetry-derived along track PWV (top) and SLA (bottom) overlapped with ONI over Pacific Ocean

The spatial plot of secondary principal component (PC2), which explains 13% and 10% of the total variance for PWV and SLA, respectively, show similar pattern to EOF PC1 with the low coefficients shifted slightly eastward and westward, respectively (see Fig. 12). However, the correspondent time series have almost zero

Abdullah *et al. Earth, Planets and Space*   *(2024) 76:34*

Page 14 of 19

Fig. 12 Principal loading map of secondary principal component from EOF analysis on the Altimetry-derived PWV (top) and SLA (bottom) for along track data over Pacific Ocean

correlations with ONI, which are −0.03 for PWV and 0.01 for SLA (Figs. 13 and 14). This is because there are apparent temporal disparities between PC2 oscillation and ONI. This indicates that there is likely to be ENSO propagation features in PC2 of PWV and SLA signals. Standard EOF is incapable in encapsulating propagating signal as a single mode, instead it captures the signals from several independent modes, resulting in low correlation of two similar variations of different phases.

However, the discrepancies are varied through the entire time series for both PWV and SLA. Thus, the time series is divided into several shorter periods and only three (labelled as a, b, and c in Figs. 13 and 14) significant oscillations during extreme ENSO are selected for cross correlations analysis. The selected period of short time series is 1.5 years before and after (3 years in total) the maximum ONI of the ENSO cycle. This range is selected as the minimum period of ENSO cycle is 2.5–3 years (Tudhope et al. 2001; McPhaden et al. 2006). The cross correlations are computed to determine the temporal

discrepancies that contribute to maximum correlations between the variables and ONI. The results in Figs. 13 and 14 show the temporal lags for maximum correlation.

The highest correlation for PWV and SLA are during ENSO cycle c, from May 2014 to April 2017, with maximum correlation −0.95 by 2 month lag and 0.87 by 8 month lag, respectively. Meanwhile, the lowest correlation for PWV is during ENSO cycle A, from May 1996 to April 1999, with maximum correlation −0.63 by 5 month lag and for SLA is during ENSO cycle B, from June 2008 to May 2011, with maximum correlation −0.58 by -5 month lag. According to these results, when compared to ONI, temporal lags for PWV and SLA are not similar and inconsistence for every cycle. Thus, it is unreliable to draw a conclusive decision whether there are ENSO propagation features in PC2 of PWV and SLA signal. There is high probability that the signal is from local variation or other phenomena, which is not significantly related to ENSO.
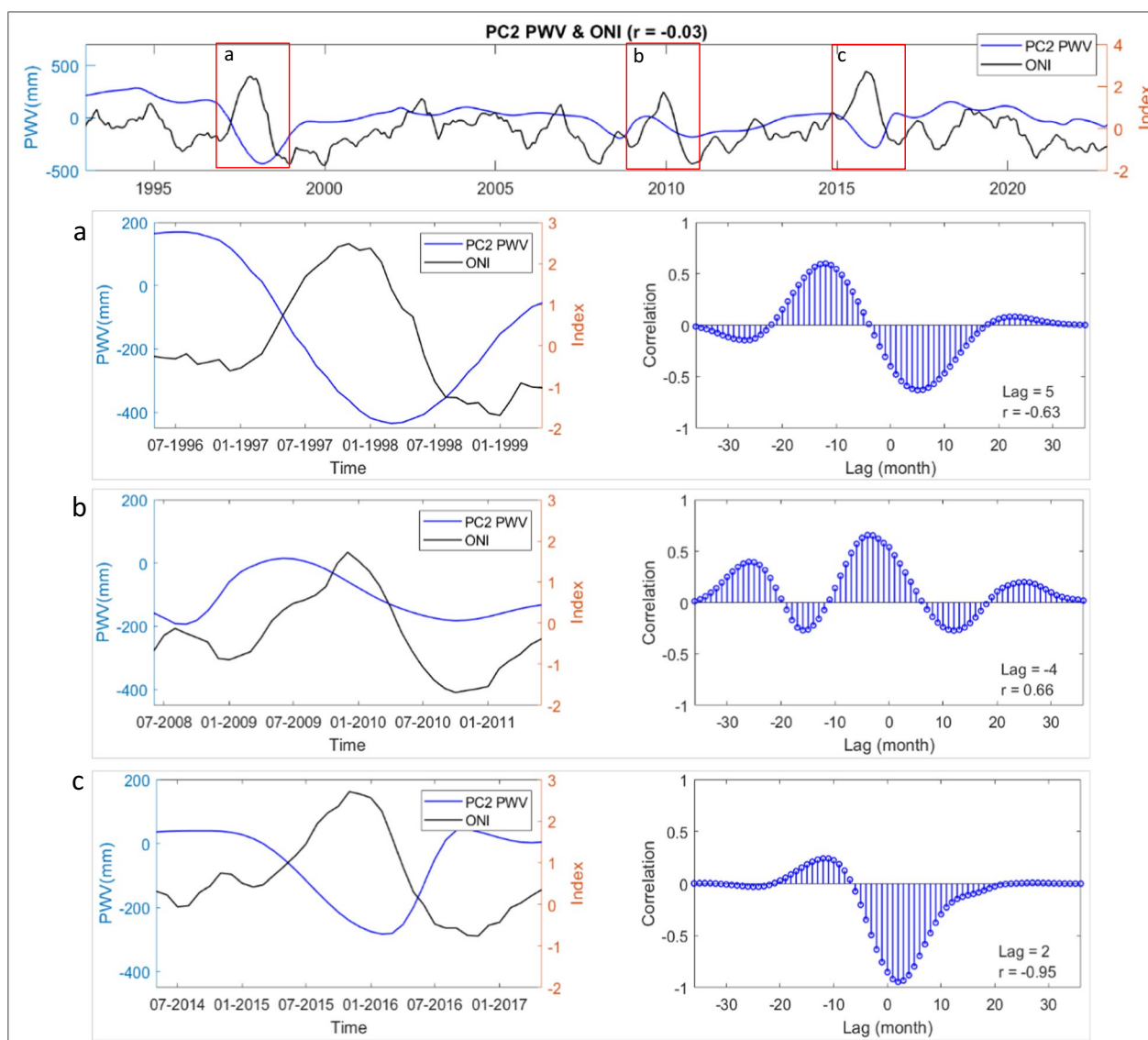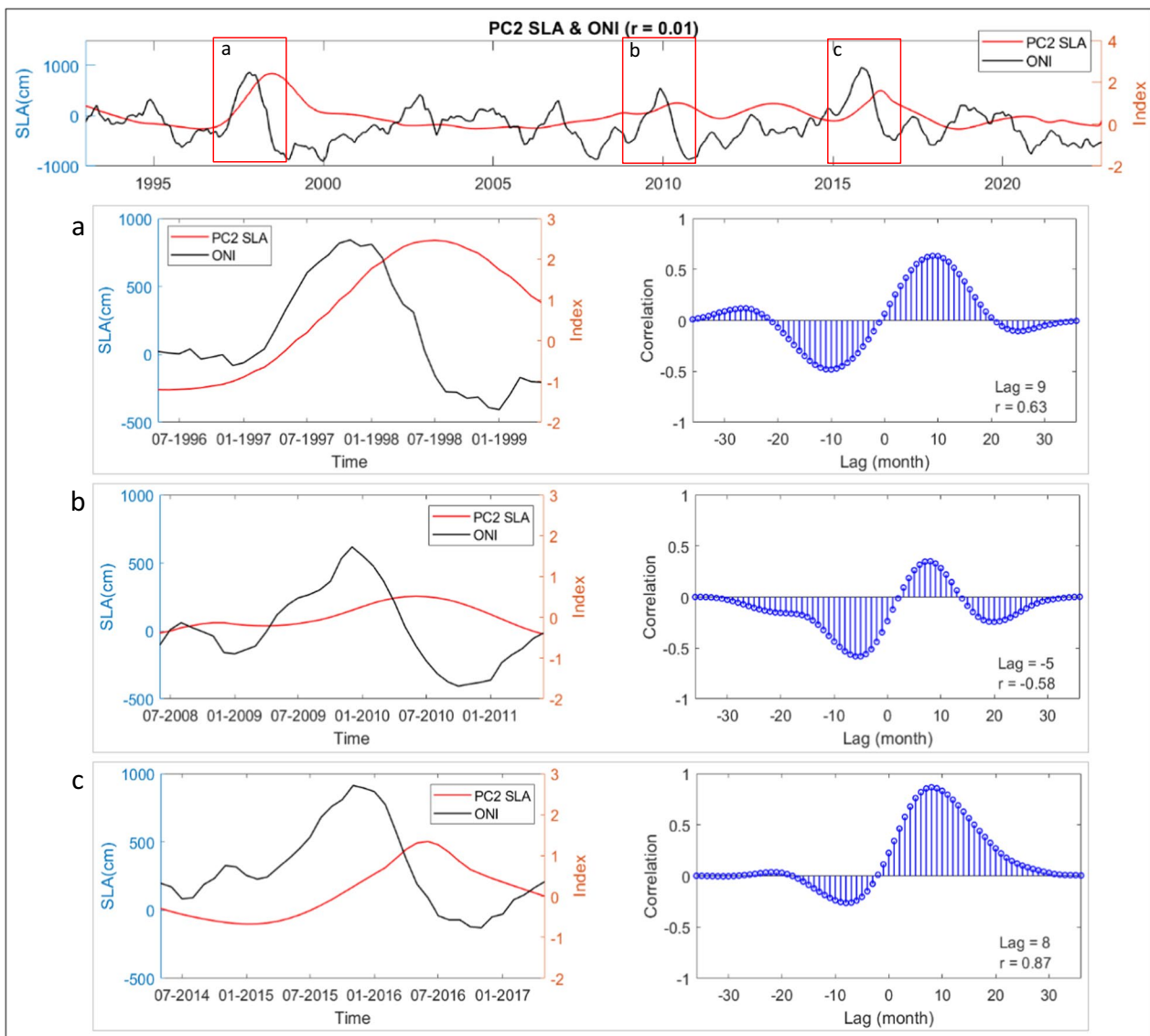
Fig. 13 Time series of secondary principal component for Altimetry-derived along track PWV overlapped with ONI and the cross correlation for selected period

Another dominant event that occurs in the Pacific Ocean is the Inter-Tropical Convergence Zone (ITCZ). As indicated in EOF spatial pattern in Fig. 12, particularly for PWV, the positive values are concentrated in the upper latitude, between 3° and 25° in the central Pacific. Although ITCZ varies seasonally, and the seasonal oscillation have been removed from the data set, however, the seasonal variations remain.

The ITCZ is defined as a cloud belt created by a high concentration of uprising air driven by the convergence of north-easterly and south-easterly trade winds (Smith 2003). The ITCZ position changes seasonally in response to the warmest area, theoretically it will travel to north during boreal summer and south during boreal winter. However, ITCZ in the eastern Pacific remains in the northern hemisphere during both seasons. This is driven by the equatorial asymmetry in SST and formation of stratus cloud in the southern Pacific, which probably prompted by the land–sea distribution (Xie and Philander 1994; Xie 1996).

However, it is too early to draw a solid conclusion that the PC2 is associated with ITCZ propagation as the assumption is only based on spatial patterns of the PWV and SLA. Further validation using other independent data (e.g., satellite imagery, precipitation, wind, etc.) with temporal propagations and more insightful analyses are

Fig. 14 Time series of secondary principal component for Altimetry-derived along track SLA overlapped with ONI and the cross correlation for selected period

required to substantiate the assumption. Nevertheless, phenomena that associate with PC2 is worth to be investigated as the percentage of total variance, particularly for PWV is rather significant (13%).

Conclusions and remarks

Comprehensive analyses have been conducted to identify and compare the interannual oscillation signature related to ENSO in altimeter-derived SLA and PWV time series. According to variability analysis across equator, the fluctuation of SLA and PWV associated well with ENSO oscillation as the increasing and decreasing anomalies spatially and temporally similar to ONI. Spatial plots also

indicate that the variation of SLA and PWV during La Niña and El Niño are parallel to the equilibrium theory of walker circulation, which is SLA and PWV anomalies are higher in the central Pacific and lower in the Maritime Continent during El Niño and conversely during La Niña. The signature of ENSO in Altimetry-derived SLA and PWV variability for 30 years is undeniably substantial as the correlations between both variables with ONI at ENSO region are acceptably high (> 0.8).

A standard EOF analysis is performed to identify the variability modes of SLA and PWV that occur in the Pacific Ocean. Two dominant modes are identified with pole-like spatial characteristics. The primary component,

PC1 for both variables fully explain the ENSO variations as they have high correlation with ONI, particularly for PWV with correlation coefficient of 0.87, and SLA with correlation coefficient of 0.80. However, for secondary component, PC2, there is no conclusive evidence that associate its oscillation with ENSO as almost zero correlations are found for both SLA and PWV. Based on the EOF pattern for PC2, the signal most probably associated with another dominant event in the Pacific Ocean, which is ITCZ.

As per these results, the capability of satellite Altimetry in observing the atmosphere through PWV derived from on-board microwave radiometer data is comparable, and even better in some cases with the altimeter-derived SLA. The variability of PWV is consistent with the ENSO interannual transition, temporally and spatially, showing that the ability of satellite Altimetry in observing atmosphere variability is as reliable and accurate as perceiving ocean geophysical oscillation. These results reinforce the confidence in the ability of satellite Altimetry for ocean–atmospheric studies.

As the satellite Altimetry capability in providing accurate sea level measurement has been recognised many years ago, and the new potential of observing atmospheric water vapour has so far shows substantially satisfactory results, the aim to optimise the satellite by utilising synchronous altimeter–radiometer measurement to observe ocean–atmosphere coupling in support of hydro-meteorological hazard mitigation is highly feasible. Altimetry satellite might not be able to measure daily weather, particularly rainfall, which highly variable through time and space, as its highest temporal resolution is approximately 9–10 days and longer data post processing. However, it is reliable enough to monitor longer periodic phenomena, such as ENSO, Indian Ocean Dipole (IOD), Madden–Julian Oscillation (MJO), and the oscillation of Inter-Tropical Convergence Zone (ITCZ), which associate with monsoon.

Using both ocean and atmosphere measurement from satellite Altimetry not only present a new potential of the satellite itself, but also a way to overcome the drawback of previous ocean–atmosphere studies, which has temporal and spatial disparities as each variable were observed using different platforms at different time and locations.

Abbreviations

AVISO	Archiving, Validation, and Interpretation of Satellite Oceanographic Data
ECMWF	European Centre of Medium Range Weather Forecast
ECMWF ERA5	European Centre of Medium Range Weather Forecast Reanalysis v5
ENSO	El Niño–Southern Oscillation
EOF	Empirical Orthogonal Function
GNSS	Global Navigation Satellite System
GPM	Global Precipitation Measurement
GPT	Global Pressure Temperature
IOD	Indian Ocean Dipole
ITCZ	Inter-Tropical Convergence Zone
MJO	Madden–Julian Oscillation
NRMSD	Normalised Root Mean Square Difference
ONI	Oceanic Nino Index
PC	Principal Component
PWV	Precipitable Water Vapour
RADS	Radar Altimetry Database System
RMSD	Root Mean Square Difference
SLA	Sea Level Anomaly
SSH	Sea Surface Height
SST	Sea Surface Temperature
STDD	Standard Deviation of Difference
SWH	Significant Wave Height
WTC	Wet Tropospheric Correction

Author contributions
DDW provide the initial ideas, design the research framework, and wrote the manuscript. NNA design the research framework, implement the research designed, perform data processing, and wrote the manuscript. IM and WK assist in supervise in data processing and analyses. ZAJT and MRA assisted in metrological discussion and analysis. FN assisted in data processing.

Availability of data and materials
Satellite altimetry data and European Centre of Medium Range Weather Forecast (ECMWF) data are available in Radar Altimeter Database System (RADS) and Archiving, Validation, and Interpretation of Satellite Oceanographic data (AVISO) ftp site (https://www.aviso.altimetry.fr/en/data/data-access/ftp.html). Oceanic Nino Index (ONI) data are available at National Oceanic and Atmospheric Administration (NOAA) website (https://origin.cpc.ncep.noaa.gov/products/analysis_monitoring/ensostuff/ONI_v5.php).

Declarations

Competing interests
The authors declare that they have no conflict of interest.

Author details
[1]Geodetic Science, Engineering and Innovation Research Group, Faculty of Earth Sciences and Technology, Bandung Institute of Technology, Bandung 40132, Indonesia. [2]Surveying and Cadastre Research Group, Faculty of Earth Sciences and Technology, Bandung Institute of Technology, Bandung 40132, Indonesia. [3]Atmospheric Science Research Group, Faculty of Earth Science and Technology, Bandung Institute of Technology, Bandung 40132, Indonesia.

References
Abdalla S, Kolahchi AA, Ablain M, Adusumilli S, et al. Altimetry for the future: building on 25 years of progress. Adv Space Res. 2021;68(2):319–63

Abdullah *et al. Earth, Planets and Space*   (2024) 76:34

Page 18 of 19

Abdullah NN, Idris NH, Maharaj AM (2016) The Retracked Sea Levels from SARAL/AltiKa satellite altimetry: the case study around the strait of Malacca and the south China Sea. Int J Geoinform 12(2):33–39

Abdullah, NN (2018) *The Optimal Coastal Retracked Sea Levels From Saral/Altika Satellite Altimetry over the Southeast Asia.* (Master of Philosophy), University of Technology Malaysia, Johor, Malaysia

Andersen OB, Scharroo R (2011) *Coastal Altimetry* (Vol. 1, pp. 103–146). London, New York: Springer

Aparna S, McCreary J, Shankar D, Vinayachandran P (2012) Signatures of Indian Ocean Dipole and El Niño-Southern Oscillation Events in Sea Level Variations in the Bay of Bengal. J Geophys Res 117:C10

Blanc F, Borra M, Boudou P (1996) AVISO User Hand-book for Merged TOPEX/POSEIDON Products. *Toulouse, France: AVI-NT-02–101-CN, Edition,* 3

Böhm J, Heinkelmann R, Schuh H (2007) Short note: a global model of pressure and temperature for geodetic applications. J Geodesy 81(10):679–683

Brown S, Ruf C, Keihm S, Kitiyakara A (2004) Jason microwave radiometer performance and on-orbit calibration. Mar Geodesy 27(1–2):199–220

Brown S (2010) A Novel Near-land Radiometer Wet Path-delay Retrieval Algorithm: application to the Jason-2/OSTM advanced microwave radiometer. *IEEE Trans Geosci Rem Sens,* 48:4. doi: https://doi.org/10.1109/TGRS.2009.2037220

Chang C, Wang Z, Ju J, Li T (2004) On the Relationship between Western Maritime Continent Monsoon Rainfall and ENSO During Northern Winter. J Clim 17(3):665–672

Chang-Yang CH, Sun IF, Tsai CH, Lu CL, Hsieh CF (2016) ENSO and frost code-termine decade-long temporal variation in flower and seed production in a subtropical rain forest. J Ecol 104(1):44–54

Chen G, Wang Z, Qian C, Lv C, Han Y (2010) Seasonal-to-decadal Modes of Global Sea Level Variability Derived from Merged Altimeter Data. Remote Sens Environ 114(11):2524–2535

Cheng Y, Hamlington BD, Plag H-P, Xu Q (2016) Influence of ENSO on the Variation of Annual Sea Level Cycle in the South China Sea. Ocean Eng 126:343–352

Cipollini P, Calafat FM, Jevrejeva S, Melet A, Prandi P (2016) Monitoring sea level in the coastal zone with satellite altimetry and tide gauges. *Surv Geophys*, 1:1–25.

Debele SE, Kumar P, Sahani J, Marti-Cardona B, Mickovski SB, Leo LS, Porcù F, Bertini F, Montesi D, Vojinovic Z (2019) Nature-based solutions for hydro-meteorological hazards: revised concepts. Classif Schem Datab Environ Res 179:108799

Eymard L, Le Cornec A, Tabary L (1994) The ERS-1 microwave radiometer. Int J Remote Sens 15(4):845–857

Fedorov AV (2008) Ocean-Atmosphere Coupling. *Oxford Comp Glob Change*, 1:369–374.

Fernandes MJ, Lázaro C (2018) Independent Assessment of Sentinel-3A wet tropospheric correction over the open and coastal ocean. Remote Sens 10(3):484

Fernandes MJ, Lazaro C, Nunes AL, Pires N, Bastos L, Mendes VB (2010) GNSS-derived path delay: an approach to compute the wet tropospheric correction for coastal altimetry. IEEE Geosci Remote Sens Lett 7(3):596–600

Fernandes MJ, Lázaro C, Ablain M, Pires N (2015) Improved wet path delays for all ESA and reference altimetric missions. Remote Sens Environ 169:50–74

Fernandes MJ, Lázaro C, Vieira T (2021) On the role of the troposphere in satellite altimetry. Remote Sens Environ 252:112149

Garden D (2014) *Climate, Science, and Colonization* (pp. 61–80): Springer

Gastineau G, Li L, Le Treut H (2009) The hadley and walker circulation changes in global warming conditions described by idealized atmospheric simulations. J Clim 22(14):3993–4013

Gómez-Enri J, Cipollini P, Gommenginger C, Martin-Puig C, Vignudelli S, Woodworth P, Benveniste J, Villares P (2008a) *COASTALT: improving radar altimetry products in the oceanic coastal area.* Paper presented at the Remote Sensing of the Ocean, Sea Ice, and Large Water Regions 2008

Gómez-Enri J, Cipollini P, Gommenginger C, Martin-Puig C, Vignudelli S, Woodworth P, Benveniste J, Villares P (2008b) COASTALT: Improving Radar Altimetry Products in the Oceanic Coastal Area. 7105, 71050J71051–71010. doi: https://doi.org/10.1117/12.802456

Gommenginger C, Thibaut P, Fenoglio-Marc L, Quartly G, Deng X, Gómez-Enri J, Challenor P, Gao Y (2011) *Coastal Altimetry* (Vol. 1, pp. 61–101). London, New York: Springer

Gupta AK, Nair SS, Sehgal VK (2009) Hydro-meteorological disasters and climate change: conceptual issues and data needs for integrating adaptation into environment-development framework. *Earth Sci India,* 2:1

Hamlington BD, Piecuch CG, Reager JT, Chandanpurkar H, Frederikse T, Nerem RS, Fasullo JT, Cheon S-H (2020) Origin of interannual variability in global mean sea level. Proc Natl Acad Sci 117(25):13983–13990

Han G, Huang W (2009) Low-frequency sea-level variability in the South China Sea and its relationship to ENSO. Theoret Appl Climatol 97(1–2):41–52

Holton JR, Dmowska R (1989) El Niño, La Niña, and the Southern Oscillation. Academic press, Cambridge

Jayawardena A (2015) Hydro-Meteorological disasters: causes, effects and mitigation measures with special reference to early warning with data driven approaches of forecasting. Procedia IUTAM 17:3–12

Ji M, Reynolds RW, Behringer DW (2000) Use of TOPEX/poseidon sea level data for ocean analyses and ENSO prediction: some early results. J Clim 13(1):216–31

Jia X, Ge J, Wang S (2016) Diverse impacts of ENSO on wintertime rainfall over the maritime continent. Int J Climatol 36(9):3384–3397

Keihm SJ, Janssen MA, Ruf CS (1995) TOPEX/Poseidon Microwave Radiometer (TMR). III. Wet Troposphere Range Correction Algorithm and Pre-launch Error Budget. IEEE Trans Geosci Rem Sens 33(1):147–161

Kumar PS, Pillai GN, Manjusha U (2014) El Nino Southern Oscillation (ENSO) impact on Tuna Fisheries in Indian Ocean. Springerplus 3(1):1–13

Lau K, Yang S (2003) Walker Circulation Encyclopedia of Atmospheric Sciences 2505:2510

Lehodey P, Bertrand A, Hobday AJ, Kiyofuji H, McClatchie S, Menkès CE, Pilling G, Polovina J, Tommasi D (2020) ENSO Impact on Marine Fisheries and Ecosystems. El Niño Southern Oscill Chang Clim 1:429–451

Luo M, Lau N-C (2020) Summer heat extremes in northern continents linked to developing ENSO events. Environ Res Lett 15(7):074042

Lyu K, Zhang X, Church JA, Hu J, Yu J-Y (2017) Distinguishing the quasi-decadal and multidecadal sea level and climate variations in the pacific: implications for the ENSO-like low-frequency variability. J Clim 30(13):5097–5117

Maiwald F, Montes O, Padmanabhan S, Michaels D, Kitiyakara A, Jarnot R, Brown ST, Dawson D, Wu A, Hatch W (2016) Reliable and stable radiometers for jason-3. IEEE J Sel Top Appl Earth Observ Rem Sens 9(6):2754–2762

McPhaden MJ, Zebiak SE, Glantz MH (2006) ENSO as an integrating concept in earth science. Science 314(5806):1740–1745

Misra V (2014) Ocean-atmosphere interaction. Encyclop Nat Resour Water Air-Vol II:798

Moon JH, Song YT, Lee H (2015) PDO and ENSO modulations intensified decadal sea level variability in the tropical pacific. J Geophys Res 120(12):8229–8237

Oliver E, Thompson K (2010) Madden-Julian Oscillation and sea level: local and remote forcing. J Geophys Res 115:1

Oliver E, Thompson K (2011) Sea level and Circulation Variability of the Gulf of Carpentaria: influence of the Madden-Julian Oscillation and the Adjacent Deep Ocean. J Geophys Res 116:2

Philander S (1985) El Niño and La Niña. J Atmosph Sci 42(23):2652–2662

Qian Y, Zhao J, Zheng S, Cao Y, Xue L (2020) Risk Assessment of the Global Crop Loss in ENSO Events. Phys Chem Earth 116:102845

Qu Y, Jevrejeva S, Williams J, Moore JC (2022) Drivers for seasonal variability in sea level around the china seas. Global Planet Change 213:103819

Rohith B, Paul A, Durand F, Testut L, Prerna S, Afroosa M, Ramakrishna S, Shenoi S (2019) Basin-wide sea level coherency in the tropical indian ocean driven by Madden–Julian Oscillation. Nat Commun 10(1):1–9

Salinger M (2013) A brief introduction to the issue of climate and marine fisheries. Clim Change 119(1):23–35

Saramul S, Ezer T (2014) Spatial Variations of Sea Level along the coast of Thailand: impacts of extreme land subsidence, earthquakes and the seasonal monsoon. Global Planet Change 122:70–81

Shum C, Ries J, Tapley B (1995) The accuracy and applications of satellite altimetry. Geophys J Int 121(2):321–336

Smith RK (2003) *Lectures on Tropical Meteorology*: Met. Inst. d. Univ, München

Sreenivas P, Gnanaseelan C, Prasad K (2012) Influence of El Niño and Indian Ocean Dipole on Sea Level Variability in the Bay of Bengal. Global Planet Change 80:215–225

Abdullah *et al. Earth, Planets and Space*   (2024) 76:34

Page 19 of 19

Srinivas K, Kumar P, Revichandran C (2005) ENSO signature in the sea level along the coastline of the Indian subcontinent. Indian J Mar Sci 34(2):225–236

Stuecker MF, Timmermann A, Jin FF, Chikamoto Y, Zhang W, Wittenberg AT, Widiasih E, Zhao S (2017) Revisiting ENSO/Indian ocean dipole phase relationships. Geophys Res Lett 44(5):2481–2492

Thibaut P, Poisson JC, Bronner E, Picot N (2010) Relative Performance of the MLE3 and MLE4 retracking algorithms on jason-2 altimeter waveforms. Mar Geodesy 33(S1):317–335. https://doi.org/10.1080/01490419.2010.491033

Timmermann A, An S-I, Kug J-S, Jin F-F, Cai W, Capotondi A, Cobb KM, Lengaigne M, McPhaden MJ, Stuecker MF (2018) El Niño-Southern Oscillation Complexity Nature 559(7715):535–545

Trott CB, Subrahmanyam B (2019) Detection of Intraseasonal Oscillations in the Bay of Bengal using Altimetry. Atmosph Sci Lett 20(7):e920

Tsonis A, Hunt A, Elsner JB (2003) On the relation between ENSO and global climate change. Meteorol Atmos Phys 84(3):229–242

Tudhope AW, Chilcott CP, McCulloch MT, Cook ER, Chappell J, Ellam RM, Lea DW, Lough JM, Shimmield GB (2001) Variability in the El Niño-Southern oscillation through a glacial-interglacial cycle. Science 291(5508):1511–1517

Valladeau G, Legeais JF, Ablain M, Guinehut S, Picot N (2012) Comparing Altimetry with Tide Gauges and Argo profiling floats for data quality assessment and mean sea level studies. Mar Geodesy 35(sup1):42–60. https://doi.org/10.1080/01490419.2012.718226

Wang B, Wu R, Fu X (2000) Pacific-east asian teleconnection: how does ENSO affect east asian climate? J Clim 13(9):1517–1536

Wang H, Liu K, Wang A, Feng J, Fan W, Liu Q, Xu Y, Zhang Z (2018) Regional characteristics of the effects of the El Niño-Southern Oscillation on the sea level in the China Sea. Ocean Dyn 68:485–495

Xie S-P (1996) Westward propagation of latitudinal asymmetry in a coupled ocean-atmosphere model. J Atmosph Sci 53(22):3236–3250

Xie SP, Philander SGH (1994) A coupled ocean-atmosphere model of relevance to the ITCZ in the Eastern Pacific. Tellus A 46(4):340–350

Xie S-P (2009) Ocean–Atmosphere Interaction and Tropical Climate. *The Encyclopedia of Life Support Systems (EOLSS)*

Zhang X, Lu Y, Thompson KR (2009) Sea Level variations in the tropical pacific ocean and the Madden–Julian Oscillation. J Phys Oceanogr 39(8):1984–1992

Zhang T, Yang S, Jiang X, Zhao P (2016) Seasonal-interannual variation and prediction of wet and dry season rainfall over the maritime continent: roles of ENSO and monsoon circulation. J Clim 29(10):3675–3695. https://doi.org/10.1175/JCLI-D-15-0222.1

Publisher's Note

Springer Nature remains neutral with regard to jurisdictional claims in published maps and institutional affiliations.

Noor Nabilah Abdullah   Is a PhD student at Institut Teknologi Bandung, currently performing research regarding ocean-atmosphere interaction using solely satellite altimetry data over the tropic regions.

Dudy Darmawan Wijaya   Is an associate professor in Geodesy with interests in application of satellite geodesy for Earth-Atmosphere observations.

Irwan Meilano   Is a professor in Geodesy with interest in natural hazard mitigation utilising geodetic space observations.

Wedyanto Kuntjoro   Is an associate professor in Geodesy with interest in application of satellite geodesy for Earth-Atmosphere observations.

Zamzam Akhmad Jamaluddin Tanuwijaya   Is a senior lecturer in Geodesy with interest in geomorphology dan hydrometeorology study particularly over tropic region.

Muhammad Rais Abdillah   Is an assistant professor in Meteorology with interest in climate and atmospheric sciences as well as tropical dynamics.